HHS Public Access

Author manuscript

Eur J Neurosci. Author manuscript; available in PMC 2022 May 01.

Published in final edited form as:

Eur J Neurosci. 2021 November ; 54(9): 7072–7091. doi:10.1111/ejn.15463.

Aromatase and non-aromatase neurons in the zebra finch secondary auditory forebrain are indistinct in their song-driven gene induction and intrinsic electrophysiological properties

Catherine de Bournonville[1], **Kyssia Ruth Mendoza**[1], **Luke Remage-Healey**[1,*]

[1]Center for Neuroendocrine Studies, University of Massachusetts, Amherst, MA 01003

Abstract

Estrogens support major brain functions including cognition, reproduction, neuroprotection, and sensory processing. Neuroestrogens are synthesized within some brain areas by the enzyme aromatase and can rapidly modulate local circuit functions, yet the cellular physiology and sensory-response profiles of aromatase neurons are essentially unknown. In songbirds, social and acoustic stimuli drive neuroestrogen elevations in the auditory forebrain caudomedial nidopallium (NCM). In both males and females, neuroestrogens rapidly enhance NCM auditory processing and auditory learning. Estrogen-producing neurons in NCM may therefore exhibit distinguishing sensory-activation and intrinsic electrophysiological profiles. Here, we explored these questions using both immunocyctochemistry and electrophysiological recordings. Immunoreactivity for aromatase and the immediate early gene EGR1, a marker of activity and plasticity, were quantified in NCM of song-exposed animals vs. silence-exposed controls. Using whole-cell patch clamp recordings from NCM slices, we also documented the intrinsic excitability profiles of aromatase-positive and aromatase-negative neurons. We observed that a subset of aromatase neurons were significantly activated during song playback, in both males and females, and in both hemispheres. A comparable population of non-aromatase-expressing neurons were also similarly driven by song stimulation. Membrane properties (i.e., resting membrane potential, rheobase, input resistance, and multiple action potential parameters) were similarly indistinguishable between NCM aromatase and non-aromatase neurons. Together, these findings demonstrate that aromatase and non-aromatase neurons in NCM are indistinct in terms of their intrinsic electrophysiology and responses to song. Nevertheless, such similarities in response properties may belie more subtle differences in underlying conductances and/or computational roles that may be crucial to their function.

Keywords

intrinsic excitability; estradiol; EGR1; Birdsong; neurosteroid

*Corresponding author.

Author contributions

CdB and LRH designed the experiments; CdB, KRM, and LRH performed the experiments; CdB and KRM analyzed the raw data; CdB and LRH wrote and edited the manuscript.

Conflict of interests: The authors declare no competing interests.

INTRODUCTION

Hormone secreting cells have intrinsic electrophysiological properties that are thought to enable the conversion of regulatory inputs into on-demand hormone release. A growing number of intrinsic and network-mediated properties have been characterized for peptidergic cells in peripheral endocrine glands, and also within the brain. For example, GnRH secretion from hypothalamic neurons depends on chloride-channel regulation (Herbison and Moenter, 2011), burst-firing release of hypothalamic vasopressin and oxytocin is NMDA- and calcium-channel dependent (Kirchner et al., 2018; Pitra et al., 2019), and a balance of voltage-gated and potassium-activated calcium conductances in pancreatic beta cells is important for insulin secretion (Braun et al., 2008).

A similar understanding of the electrophysiological properties of steroid-producing cells in the body is currently lagging, and in particular for neurosteroid synthesizing cells in the brain. Two identified properties, low voltage-gated calcium channels as well as calcium-activated potassium channels, are enriched in adrenal glomerulosa cells (i.e., those that secrete corticosteroids) and ovarian granulosa cells (i.e., those that secrete sex steroids). These ionic conductances have been linked to steroidogenesis in these two canonical endocrine organs (Agoston et al., 2004; Hattangady et al., 2016; Kunz et al., 2007a; Traut et al., 2009). For cells that synthesize steroids in the brain, such as neurons that express aromatase (estrogen synthase; (Cornil et al., 2004)), it is possible that similar intrinsic electrophysiological properties obtain, and are distinct from non-aromatase neurons embedded in the same brain regions (Billing et al., 2020). One step toward testing this hypothesis is to examine the response properties of aromatase+ vs aromatase- neurons in an identified circuit in which these neurons are known to have significant functions.

Neuroestrogens are important neuromodulators that regulate social communication and other sexual behaviors (Balthazart et al., 2018; Cornil and de Bournonville, 2018; de Bournonville et al., 2017; Vahaba and Remage-Healey, 2018). The production and local action of neuroestrogens is key for auditory processing in songbirds. The auditory forebrain in songbirds expresses high levels of neuronal aromatase (Ikeda et al., 2017; Saldanha et al., 2000). Hearing songs from conspecifics induces immediate-early gene expression within the caudomedial nidopallium (NCM) of the auditory pallium of songbirds (e.g. (Krentzel et al., 2020; Mello and Ribeiro, 1998; Moorman et al., 2011)) and estrogens can enhance song selectivity in this region (Maney et al., 2006). Song-induced immediate early gene expression is specific to conspecific vocalizations (Bailey and Wade, 2005) and is related to previous experience (Bolhuis et al., 2000). Secondary auditory areas in which these responses occur, such as NCM or CMM, are thus key regions for the perceptual processing of salient stimuli. Neuroestrogens produced in NCM are thought to be important for this process. Song-induced EGR1 expression is attenuated after acute estrogen synthesis blockade (Krentzel et al., 2020) consistent with a dependent regulation by local aromatase activity. Neuroestrogens are rapidly synthesized within NCM of both males and females in response to song (Remage-Healey et al., 2012, 2008) and estrogens can directly enhance the auditory-evoked activity of NCM neurons (Remage-Healey et al., 2010; Remage-Healey and Joshi, 2012). In males, neuroestrogen synthesis is likely de novo in NCM (Schlinger et al., 1992), while in females hearing song induces a local production of testosterone that

is immediately converted into estradiol to regulate song processing (de Bournonville et al., 2020). Furthermore, in males, infusing an aromatase inhibitor in NCM rapidly disrupts song phonotaxis (Remage-Healey et al., 2010) and the formation of new associations between sounds and behaviorally relevant consequences (Macedo-lima and Remage-healey, 2020a). Therefore, in both males and females, NCM aromatase neurons are pivotal for processing auditory inputs from the environment to guide behavioral responses.

Despite an increasing understanding of neuroestrogen synthesis and action in a variety of species and brain areas (Balthazart et al., 2018), the specific activation of aromatase neurons in response to sensory stimuli has not been resolved. Furthermore, aromatase cells have been shown to have specific electrophysiological properties (e.g. aromatase neurons from the amygdala in mice, (Billing et al., 2020)). Yet despite their central role, the firing phenotype of aromatase neurons within NCM has never been formally studied. In this study, we combined immunostaining and whole-cell patch clamp in order to elucidate answers to these questions.

METHODS

Animals

Adult (> 105 dph) Male and female zebra finches (*T. guttata*) were used for this study. Protocols were approved by the Institutional Animal Care and Use Committee at the University of Massachusetts. All animals were raised from our colony or came from a commercial supplier.

Stimulus presentation

The day before song stimulation, zebra finches were moved to individual cages inside sound-attenuated chambers (Eckel Industries) equipped with a speaker. Song stimulation and tissue collection was performed the next morning. Control animals were exposed to silence (n = 3, one male and two females), and a total of 6 males and 6 females were exposed to songs. Song stimulation consisted of 1-min recording of intermittent male song from 3 individual males, repeatedly looped for a total duration of 30 minutes. Stimuli were band-pass filtered (2–12 kHz, identical procedures in (Remage-Healey et al., 2012, 2008)) and were played back through the speaker inside each chamber at a maximum level of 70 dB measured at the bird's cage. The stimuli used were songs recorded from another colony and were known to induce EGR1 expression (Krentzel et al., 2020), evoked changes in NCM neuron activity (Remage-Healey et al., 2013, 2010) and estradiol elevation (Remage-Healey et al., 2012, 2008). The stimulus presentation was followed by 50 minutes of silence to allow egr1 induction (Krentzel et al., 2020).

Perfusion and brain sectioning

Eighty minutes following the onset of the song playback, birds were euthanized by isoflurane overdose and transcardially perfused with 0.1M phosphate buffer (PB) with 0.9% saline (PBS) followed by 4% paraformaldehyde (PFA). The timing was calculated for the PFA to fix the brain almost exactly ninety minutes after the onset of stimulus presentation since it correspond to the peak of song-induced EGR1 expression (Mello and Ribeiro,

1998). The brains were collected, post-fixed in 4% PFA at room temperature for 2 hours, and submerged in 20% sucrose PB in 4°C overnight. The brains were then molded in OCT compound and sectioned sagittally at 35 μm using a cryostat (Leica, Germany). The sections were kept at −20°C in cryoprotectant (30% sucrose, 30% ethylene glycol, 1% polyvinylpyrrolidone in PB) until processed for immunostaining.

Immunostaining

Brain sections were rinsed with PB, permeabilized and blocked with 10% donkey serum in 0.3% PB Triton X (PBT) for two hours at room temperature. The sections were then incubated in primary antibodies in 0.3% PBT at 4°C for 48 hours. The polyclonal rabbit anti-EGR1 (Santa-Cruz biotechnology sc-189, 1:500) and the monoclonal mouse anti-NeuN (Millipore MAB377, 1:2000) were previously used to stain telencephalon tissue in numerous songbirds studies (e.g. (Chen et al., 2017; Ikeda et al., 2017; Zengin-toktas and Woolley, 2017)). The polyclonal sheep anti-aromatase (Bethyl labs, 1:2000) was generated against the 3' end of the zebra finch aromatase coding region and was previously used in zebra finch diencephalon (Kabelik et al., 2011). Following the primary incubation, sections were washed three times in 0.1% PBT and were incubated in secondary antibodies in 0.3% PBT (Alexa conjugated donkey anti-rabbit 594, donkey anti-sheep 488, donkey anti-mouse 647; Thermo Fisher Scientific Inc., MA; all 1/200) for 1 hour at room temperature. The sections were then washed three times in 0.1% PBT, mounted onto gelatin-coated slides and cover slipped using ProLong Diamond Antifade Mounting Medium (Thermo Fisher). Different runs of immunostaining were processed, each one included at least one animal of every conditions (male vs. female; silence vs. song-exposed). A subset of animals were also used to evaluate the specificity of the sheep anti-aromatase antibody. Using the same protocols as above, these sections were stained with both the sheep anti-aromatase antibody as above and a polyclonal rabbit anti-aromatase antibody (gift from Dr. Saldanha, 1:2000) that was validated and used extensively in zebra finch tissue (Ikeda et al., 2017; Rohmann et al., 2006; Saldanha et al., 2000). The co-expression between both antibodies was assessed.

Image analysis and quantifications

Sections were imaged using a confocal microscope (NA1, Nikon, Tokyo, Japan) with NIS-Elements imaging software (Ar; RRID: SCR_002776) in the UMass Nikon Center for Excellence housed in the Institute for Applied Life Sciences. The laser strength and gain were kept consistent across sections and sub-regions. Pictures of the ventral and dorsal NCM were taken as in (Ikeda et al., 2017). Stich images using 10X magnification were first taken to observe the overall pattern of staining and structures (using NeuN staining). The specific lobule-shape of NCM was observed in sections ~ 0.2–1.0 mm from the midline and was defined by thickness of the hippocampus and the absence of nucleus taenia (large NeuN positive cells and dense aromatase staining; Figure 1) as previously described (Ikeda et al., 2017). Once subregions were identified, images using 60X magnification and z-stack settings (1μm z-steps for 15 μm) were taken. Specifically, dorsal (NCMd), medial (NCMm) and ventral NCM (NCMv) were imaged in up to 6 sections of NCM (up to 3 in each hemisphere), either medially (when the boundary between CMM, Field L and NCM is apparent) or caudally (when NCM is more round in shape medially and Field L not discernable anymore). The total number of cells (DAPI-positive nuclei), the number of

EGR1 positive and aromatase positive neurons was manually quantified in each unprocessed z-stack image by an experimenter blind to the treatment using the cell counter tool in FIJI software (National Institutes of Health, USA, RRID: SCR_002285). The percentage of aromatase and EGR1 positive cells was calculated by dividing the number of these cells by the total number of cells. The co-expression was calculated by dividing the number of cells expressing both antibodies by the total number of aromatase positive cells. All statistical analyses were performed using GraphPad Prism 6.01 (GraphPad, LaJolla, CA, USA). The main goal of this study focused on lateralization, sex, and NCM topography effects on song-activated cells while the song stimulation was confirming the validity of our testing conditions and has been well characterized by many studies (e.g. (Maney et al., 2006; Mello and Ribeiro, 1998; Sanford et al., 2010)). For this reason, only 3 animals were exposed to silence while 12 animals were exposed to song. Main effects (lateralization, sex, topography) were thus assessed only in song-primed animals using t tests and ANOVAs while the song stimulation effect was assessed by non-parametric stats (Mann-Whitney U tests) due to the low number of subjects in the control group.

Brain slices and Whole-cell Patch-clamp

In order to study the intrinsic properties of aromatase neurons vs. non-aromatase neurons, neurons were recorded *in vitro* in NCM slices, similar to prior work in the lab (Spool et al., 2021). A total of 35 adult males and female zebra finches were used and a final number of 81 neurons were included in the analysis. Zebra finches were killed by rapid decapitation and their brains were collected and immersed in ice-cold cutting solution (224 mM glycerol, 25 mM NaHCO3, 2.5 mM KCl, 1.25 mM NaH2PO4, 25 mM glucose, 0.5 mM CaCl2, and 3 mM MgCl2, 0.4 mM ascorbic acid, 2 mM na pyruvate, 3 mM myo-inositol; 310 mOsm; pH 7.4 when saturated with 95% O2 / 5% CO2). Brains were cut sagittally using a vibratome (VT1000S, Leica Biosystems Inc.) in 250–300μm thick sections. Previous studies based on electrophysiology and immediate early gene expression (Dagostin et al., 2015; Mello and Clayton, 1994) reported the lateral boundaries of NCM at around ~1 mm from the midline, thus the current study included the three first sections following the midline (~750 μm). Sections were immediately transferred to aCSF external solution (37°C; 112 mM NaCl, 25 mM NaHCO3, 2.5 mM KCl, 1.25 mM NaH2PO4, 25 mM glucose, 2 mM CaCl2, and 1 mM MgCl2, 0.4 mM ascorbic acid, 2 mM na pyruvate, 3 mM myo-inositol; 310 mOsm; pH 7.4 when saturated with 95% O2 / 5% CO2) and stayed in these conditions for 30 minutes before being transferred in bubbled aCSF at room temperature for the experiment.

For the recordings, slices were transferred to a recording chamber mounted on the stage of a fixed stage microscope (Eclipse FN1; Nikon) that was equipped with a water emersion objective (CFI Fluor; 40X; NA = 0.8; WD = 2.0 mm; Nikon). Neurons were imaged using a charge-coupled camera (QIClick; QImaging) using DIC optics, and the slices were continuously perfused with bubbled aCSF. Glass pipettes were pulled from borosilicate glass tubes using a two-stage, vertical puller (PC-10, Narishige International USA). When backfilled with internal solution (110 mM K-gluconate, 30 mM KCl, 1 mM MgCl2, 10 mM HEPES, 0.2 mM EGTA, 2 mM Mg-ATP, 0.5 mM GTP, 10 mM Na2-phosphocreatine; 349 mOsm; pH 7.4), the measured tip resistance was 4–7 MΩ. Once whole-cell configuration was achieved, cells were allowed to stabilize during five minutes before data collection. All

neurons that showed changes by more than 20% from baseline values in series resistance were removed from the analysis. Similarly, cells showing changes in rheobase (more than 20% compared to baseline) during the recording period were removed from the analysis. All signals were acquired in current-clamp mode with neurons kept at their resting membrane potential (RMP) in order to assess neuronal electrphysiological properties. Stimulations consisted of step hyperpolarizing and depolarizing current injections (500–2000 ms) at intervals of 10 or 20 pA relative to baseline holding current. Experimental data were acquired at 40 kHz using multi-channel acquisition software (PATCHMASTER; HEKA Elektronik), digitized using a patch clamp amplifier (EPC 10 USB; HEKA Elektronik), then exported to Igor Pro (WaveMetrics; RRID: SCR_000325) and processed using a 1 kHz low-pass filter.

After recordings were completed, the recording pipette was slowly removed, and slices were drop-fixed overnight in 4% paraformaldehyde in PB. They were finally transferred in cryoprotectant and kept at −20 °C until processed for immunostaining.

Identification of recorded neurons and aromatase immunostaining

The combination of Alexa and neurobiotin contained in the microelectrodes allowed the subsequent identification of recorded neurons (Figure 7). For immunostaining, brain sections were rinsed with PB, permeabilized and blocked with 10% normal goat serum in 0.3% PB Triton X (PBT) for two hours at room temperature. The sections were then incubated in the polyclonal rabbit anti-aromatase antibody (see immunostaining section; 1:2000) in 0.3% PBT at 4°C for 48 hours. Following the primary incubation, sections were washed three times in 0.1% PBT and were incubated in both Alexa goat anti-rabbit 594 (Thermo Fisher Scientific Inc., MA; 1/200) and dylight 488 streptavidin (Vector Laboratories SA-5488; 1/200) for 1 hour at room temperature. The sections were then washed three times in 0.1% PBT, mounted onto gelatin-coated slides and cover slipped using ProLong Diamond Antifade Mounting Medium (Thermo Fisher).

Sections were imaged using a confocal microscope (NA1, Nikon, Tokyo, Japan) with NIS-Elements imaging software (Ar; RRID: SCR_002776). On each section, the recorded neuron was identified by the visualization of Alexa 488. Z-stack 60X magnification images were taken from the one edge of the neuron to the other (1μm z-steps for 10–25 μm) The coexpression between alexa 488 (patched neuron) and alexa 594 (aromatase) was assessed manually for each neuron.

Data analysis

Recordings were analyzed using Igor Pro (Wavemetrics, Lake Oswego, OR, USA) and Patcher's Power Tools macros (PPT; Max-Planck Institute for Biophysical Chemistry, Gottingen, Germany). Voltage-Current (VI) relationships were constructed based on negative potentials to −50 mV. Input resistance (R_i) was calculated from the slope of the VI curve. Rheobase represented the minimum positive current amplitude that elicited an action potential. Number of action potentials was defined as the maximum number of action potentials evoked by any current step for that cell. Then the following measurements analyzed the characteristics of the first action potential by current injection (i.e. at rheobase,

see Figure 6E): The membrane time constant (Tau) was calculated by fitting a single exponential function to the decay of the repolarization phase of the membrane potential; Peak amplitude was defined as the maximal voltage of the first evoked action potential; Peak latency was calculated as the time between the start of the stimulus and the first action potential threshold; Peak half-width (HW) was the duration (msec) at the point of half the amplitude measured from the threshold to the peak. Finally, the slope of the evoked firing rate to positive current curve (FI slope) was calculated from the first current that evoked an action potential to the first current that generated the maximum evoked firing rate (Meitzen et al., 2009). Data are presented as mean ± SEM. All statistical analyses were performed using GraphPad Prism 6.01 (GraphPad, LaJolla, CA, USA). The firing phenotype of neurons was first analyzed as in (Dagostin et al., 2015) to discriminate among tonic, transient and phasic cells using one-way ANOVAs. Since the firing pattern was significantly different between these three types of cells, other analyses were conducted separately within each cell type. Differences between sex or between aromatase-positive vs. aromatase-negative neurons were assessed by one-way ANOVAs.

RESULTS

1.1. Aromatase and EGR1 immunostaining

1.1.1. Song-induced EGR1 and aromatase expression—The immunostaining and the electrophysiological experiments both targeted aromatase neurons but used two different antibodies, thus we first confirmed the co-expression of both anti-aromatase antibodies in different brain regions (See supplementary information and Figure S1). To identify whether aromatase cells were activated during auditory processing, aromatase (Figure 2A,D), EGR1 (Figure 2B,D) as well as its co-expression (Figure 2C,F) were quantified in NCM sections of animals exposed to silence (Figure 2A–C) versus animals exposed to song (Figure 2D–F). In agreement with previous studies (see Discussion), the data confirmed a strong increase in EGR1 expression induced by song, i.e. a significantly higher number of EGR1 cells in song-exposed animals as compared to silence-exposed controls ($U_{(n1=3, n2=12)} = 3.0$, $p = 0.031$; Figure 2H). The number of aromatase cells was not significantly different between treatments ($U_{(n1=3, n2=12)} = 10.0$, $p = 0.255$; Figure 2G). We furthermore demonstrated a higher number of EGR1 cells within aromatase positive cells in song-primed animals compared to silence-primed animals ($U_{(n1=3, n2=12)} = 4.0$, $p = 0.044$; Figure 2I). The number of EGR1 cells in non-aromatase neurons also tended to be higher in song-primed animals as compared to controls ($U_{(n1=3, n2=12)} = 6.0$, $p = 0.088$; Figure 2J).

The difference between males and females in the auditory response was also quantified in the current study. In this case, the number of aromatase positive cells (Figure 3A, D), EGR1 positive cells (Figure 3B, E) and the co-expression (Figure 3C, F) was counted and compared between sexes. The EGR1 expression and its coexpression with aromatase were analyzed only in song-primed animals while the aromatase expression was analyzed in all animals (including silence-exposed animals) since song-stimulation has no predicted effect on aromatase expression within this timescale. The data did not show any significant differences between males and females either for the number of aromatase cells ($t_{13} = 0.995$, $p = 0.338$; Figure 3G) or for the song-induced EGR1 expression ($t_{10} = 0.745$, $p = 0.474$;

Figure 3H). A similar result was obtained for the activation of aromatase positive neurons in NCM during song stimulus (t_{10} = 1.172, p = 0.268; Figure 3I).

We next compared the topography of auditory-evoked activation and aromatase cells within different domains of NCM. The number of aromatase positive cells (Figure 4A, D), EGR1 positive cells (Figure 4B, E) and the co-expression (Figure 4C, F) was quantified and compared between the dorsal, medial and ventral NCM. For reasons stated above, the EGR1 expression and its coexpression with aromatase were analyzed only in song-primed animals while the aromatase expression was analyzed in all animals. The number of cells positive for aromatase or EGR1 was different depending on the subregions of NCM ($F_{(2, 42)}$ = 4.58, p = 0.016; $F_{(2, 33)}$ = 3.76, p = 0.034 respectively). Specifically, a higher number of aromatase cells was observed in the ventral part of NCM as compared to the dorsal part (see Figure 4G; Tukey post hoc comparison p = 0.016). By contrast, the number of NCM neurons showing EGR1 expression was higher in the dorsal part of NCM as compared to the ventral part (see Figure 4H; Tukey post hoc comparison p = 0.036). Similarly, the number of aromatase neurons with EGR1 co-expression was also different in the three subregions ($F_{(2, 33)}$ = 4.64, p = 0.017), i.e. higher in the dorsal NCM compared to the ventral NCM (see Figure 4I; Tukey post hoc comparison p = 0.020). To test whether these differences in EGR1 expression between subregions could be due to a higher density of cells, we checked for region differences in the DAPI staining. The analysis revealed a main effect of subregions ($F_{(2, 42)}$ = 8.64, p < 0.001), with a higher number of DAPI nuclei in the dorsal NCM as compared to the medial NCM (Tukey post hoc comparison p = 0.042) as well as the ventral NCM (Tukey post hoc comparison p < 0.001).

The influence of cerebral hemisphere was also assessed by comparing aromatase (Figure 5A, D), EGR1 (Figure 5B, E), and their co-expression (Figure 5C, F) in the left and in the right NCM. As above, the EGR1 staining and its coexpression with aromatase were analyzed only in song-primed animals while the aromatase expression was analyzed in all animals. No statistically significant difference between hemispheres was observed in any of the measurements, i.e. in the number of aromatase cells (t_{11} = 0.820, p = 0.430; Figure 5G), in the number of EGR1 cells (t_8 = 0.929, p = 0.380; Figure 5H), or in the number of aromatase cells expressing EGR1 (t_8 = 0.259, p = 0.803; Figure 5I).

In summary, song playback induced a strong activation of NCM aromatase neurons, comparable to other NCM neuronal populations. The overall activation and the specific patterns of response in aromatase neurons were higher in the dorsal NCM as compared to the ventral NCM. No difference was observed between sexes and between hemispheres.

1.2. Whole cell patch clamp recordings

Our categorization of NCM electrical phenotypes was guided by and largely replicated a previous study (Dagostin et al., 2015) showing three main firing phenotypes observed in NCM neurons, i.e. tonic, transient, and phasic firing pattern. In agreement with this earlier work, we observed that NCM neuronal ‘types’ fell into these three main categories based on action potential number as well as accommodation profile (see representative traces in figure 6A–D). We sorted the cells based on the number of action potentials observed in response to current steps. We then confirmed that intrinsic properties differed among these phenotypes.

Confirming previous data (Dagostin et al., 2015), rheobase, input resistance, threshold and firing latency were different among the three firing phenotypes ($F_{(2,78)} > 4.490$, $p < 0.014$) while resting membrane potential, peak amplitude and Half width did not differ (Figure 6E–L; $F_{(2,78)} < 1.877$, $p > 0.16$). In summary, evoked firing of tonic cells was higher in frequency, was triggered with lower current amplitude and occurred after longer latencies than phasic cells, while transient cells showed an intermediate phenotype (details from Tukey's post hoc comparisons are shown in figure 6). Because we found reliable differences among these three phenotypes, the characterization of aromatase expression, as well as the sex and hemisphere effects were each assessed via independent analyses within each cell phenotype.

1.2.1. Intrinsic properties of aromatase positive vs. aromatase negative neurons: After the identification of aromatase staining in recorded neurons (Figure 7), intrinsic properties were found to be largely similar between aromatase vs. non-aromatase neurons in NCM (Table 1). First, we observed that aromatase neurons could be recovered within all three major electrophysiological phenotypes in NCM (tonic, transient, and phasic), and their proportion within each phenotype was largely similar. Within each firing phenotype, we observed no significant differences between aromatase-positive and aromatase-negative neurons concerning resting membrane potential (Tonic, $t_{32} = 0.361$, $p = 0.72$; Transient, $t_{28} = 0.562$, $p = 0.578$; Phasic, $t_{15} = 1.246$, $p = 0.232$), rheobase (Tonic, $t_{32} = 0.933$, $p = 0.358$; Transient, $t_{28} = 0.017$, $p = 0.986$; Phasic, $t_{15} = 0.757$, $p = 0.461$), input resistance (Tonic, $t_{32} = 0.039$, $p = 0.969$; Transient, $t_{28} = 0.057$, $p = 0.955$; Phasic, $t_{15} = 0.840$, $p = 0.414$), threshold (Tonic, $t_{32} = 1.013$, $p = 0.319$; Transient, $t_{28} = 1.013$, $p = 0.320$; Phasic, $t_{15} = 0.006$, $p = 0.995$), peak amplitude (Tonic, $t_{32} = 1.416$, $p = 0.166$; Transient, $t_{28} = 1.726$, $p = 0.095$; Phasic, $t_{14} = 0.098$, $p = 0.924$), peak latency (Tonic, $t_{32} = 0.686$, $p = 0.498$; Transient, $t_{28} = 0.020$, $p = 0.984$; Phasic, $t_{15} = 0.791$, $p = 0.441$), peak half width (Tonic, $t_{32} = 1.156$, $p = 0.256$; Transient, $t_{28} = 0.488$, $p = 0.629$; Phasic, $t_{15} = 0.869$, $p = 0.398$) or Tau (Tonic, $t_{32} = 1.250$, $p = 0.220$; Transient, $t_{28} = 1.029$, $p = 0.312$; Phasic, $t_{15} = 0.346$, $p = 0.734$). We only observed that within transient cells, aromatase-positive neurons showed a higher number of action potentials than aromatase-negative neurons ($t_{28} = 2.808$, $p = 0.009$), while it was not the case for tonic cells ($t_{32} = 0.394$, $p = 0.696$; phasic cells are defined by ultra-low intrinsic firing states, making this comparison for phasic cells moot). A more detailed examination of the FI (frequency/current) plot of NCM transient neurons (Figure 8) did not reveal any systematic nor significant differences between aromatase-positive and aromatase-negative neurons (Mean firing rate, $F_{(1,28)} = 0.072$, $p = 0.790$). Therefore, we could not attribute any passive or active membrane property of aromatase neurons in NCM that distinguished them from non-aromatase neurons.

1.2.2. Intrinsic properties of neurons from males and females—Comparison between males and females did not reveal any significant differences concerning any of the parameters analyzed (i.e. resting membrane potential, rheobase, input resistance, threshold, peak amplitude, peak latency, peak half width or Tau; Tonic, $t_{32} < 1.693$, $p > 0.100$; Transient, $t_{28} < 1.688$, $p > 0.103$; Phasic, $t_{15} < 1.666$, $p > 0.116$. *Data not shown).

1.2.3. Intrinsic properties of neurons from left and right NCM—Finally, hemisphere differences were not observed in any of the previously cited parameters within transient ($t_{28} < 1.494$, $p > 0.146$) and phasic cells ($t_{13} < 1.376$, $p > 0.192$). Tonic cells, however, showed some lateralized features, with a smaller action potential duration and a tendency to recover faster to steady state in the left hemisphere as compared to the right (Half width, $t_{30} = 2.046$, $p = 0.0496$; Tau, $t_{30} = 1.912$, $p = 0.065$). Other measures of tonic cells did not differ between hemispheres ($t_{30} < 1.286$, $p > 0.208$).

DISCUSSION

Neuroestrogens in NCM

This work extends our understanding of the role of neuroestrogens in the sensory forebrain in two significant ways. First, a substantial proportion of NCM aromatase cells were activated by auditory stimuli (15–16% of ARO cells expressed EGR1), but in apparent lockstep with non-aromatase NCM neurons. Second, aromatase neurons on the whole exhibited intrinsic passive and active membrane properties that were indistinguishable from non-aromatase neurons in NCM. Thus, our findings with electrophysiology and activity-dependent gene expression both demonstrate that, to the extent that aromatase neurons within NCM are important for local sensory (song) processing, NCM aromatase neurons are embedded in a sensory processing network and, at least *in vitro*, do not necessarily exhibit distinctive features within the larger network. The neuronal activation as well as physiology of aromatase cells are discussed below in detail in the context of sex similarities, NCM subregions, and lateralization.

Physiology of NCM neurons

This work replicated an earlier patch clamp recording study that characterized three different firing phenotypes in NCM neurons (Dagostin et al., 2015), i.e. tonic cells that sustain responses to depolarizing step currents, transient cells that produce a few action potentials at the onset of the stimulation and show modest accommodation, and phasic cells that strongly accommodate by producing a single action potential in response to all amplitude current steps. Similar categorizations have also been documented in the zebra finch auditory caudal mesopallium (Chen and Meliza, 2018) and in nuclei controlling song production (Dutar et al., 1998). The functional and computational role of each cell type, as defined by these differential accommodation phenotypes, is likely to differ in parallel. The tuning properties of sensory neurons from primary auditory areas such as field L specialize in temporal and spectral modulations in song (Woolley et al., 2009) and the secondary auditory areas such as NCM and CM receive projections from field L (Vates et al., 1996). Interestingly, the different cell types observed in CM also show temporal properties that appear to match the temporal modulation rates of zebra finch songs (Chen and Meliza, 2018). These data suggest that the three major phenotypes found in secondary auditory centers such as CM and NCM might be specialized for processing temporally-variant acoustic features. The phenotype of accommodation to depolarizing current injection appears to be highly labile when recordings continue for tens of minutes in NCM neurons, making their categorization dynamic and subject to modulation (Dagostin et al., 2015). Studying the dynamics of these processes and the potential mechanisms that modulate cell firing phenotypes would be of

great interest since almost no data are available to date. A recent study showed the role of dopamine receptor activation on song processing in NCM (Macedo-Lima et al., 2021), and that the dopamine D1-like receptors are co-expressed with aromatase in NCM neurons. Therefore, dopamine is likely to modulate the activity of aromatase neurons in the context of song processing. The current study was conducted in order to define whether basic intrinsic properties of NCM neurons would differ depending on their capacity to produce estrogens, but modulatory mechanisms such as dopamine and estradiol signaling should be tested to further clarify this work. Also, observing how the subthreshold activity of NCM neurons would change in response to song stimulation *in vivo* could be accomplished by intracellular recordings in awake animals (e.g. Vallentin et al., 2016).

This study highlights how aromatase neurons share similar intrinsic properties with non-aromatase neurons in NCM. Given the proportion of aromatase neurons activated during song processing (15–20%), measuring the intrinsic properties of aromatase neurons specifically activated by song (expressing EGR1 or recorded online) could provide specific information about their song processing dependent activity. A limitation of the current design is that the timing of song priming (song induced EGR1 expression peaks between 1 and 2 hours and is back to zero after 4 hours (Mello and Ribeiro, 1998)) and subsequent patch-clamp recordings (sections are maintained for hours *in vitro*) on these same ‘activated’ neurons is difficult to perform. Effective discrimination between activated aromatase neurons and non-activated aromatase neurons would also be difficult since these experiments use a snapshot of the EGR1 expression pattern (perfusion occurs 90 minutes after song stimulation) and thus are likely underestimate the number of EGR1 expressing cells, i.e. those that are induced after 90 minutes.

Sex differences and similarities

The current study confirmed the absence of sex difference for aromatase expression in NCM (Ikeda et al., 2017; Saldanha et al., 2000) as well as for song-induced EGR1 expression (e.g. (Avey et al., 2005; Lampen et al., 2014; Scully et al., 2017) among others). Furthermore, we show here a similar degree of song-dependent activation of aromatase cells in males and females. The concordant activation profile of aromatase neurons in the NCM of both males and females comports with the similar degree of local and acute elevation of estradiol in NCM of both males (Remage-Healey et al., 2008) and females (de Bournonville et al., 2020; Remage-Healey et al., 2012) in response to song. Furthermore, song induction of NCM neuronal activation has been shown to be dependent on aromatase activity to a similar extent in males and females (Krentzel et al., 2020). Together, these data indicate that the electrical activity of aromatase neurons, and, presumably, local neuroestrogen production, are important for sensory neuronal processing of song similarly in the brain of both males and females. The downstream consequences of elevations in NCM estradiol levels has been well characterized in males and, to some extent, in females, and include enhancing auditory response properties of NCM and HVC neurons (Krentzel et al., 2018; Remage-Healey et al., 2010; Remage-Healey and Joshi, 2012) as well as controlling song preference and discrimination (Macedo-lima and Remage-healey, 2020b; Remage-Healey et al., 2010).

Despite a similar pattern of neuroestrogen regulation of auditory representations in male and female zebra finches, this does not necessary mean that this occurs via the same mechanism. Indeed, male and female NCM express similar level of somal aromatase (Ikeda et al., 2017; Krentzel et al., 2020; Saldanha et al., 2000). However, aromatase activity is higher in males compared to females in synaptic fractions of posterior telencephalon (Rohmann et al., 2006). Interestingly, telencephalic aromatase activity is rapidly regulated by phosphorylating conditions in zebra finches, particularly within synaptosomes (Comito et al., 2016; Cornil et al., 2012). A line of work in Japanese quail has shown that aromatase activity is also sensitive to environmental stimulation (sex interaction or stress) in both males and females (Cornil et al., 2005; de Bournonville et al., 2017, 2013; Dickens et al., 2014, 2011). These effects occur within very short time scales (2–5 minutes). Thus, while the current study highlights a highly similar role for NCM aromatase neurons in auditory processing in both male and female zebra finches, further sex-specific regulation in response to song might occur within shorter time scales and within specific subcellular compartments, such as at the synapse itself.

Finally, it is possible that the absence of sex-specific neuronal activation was due to the stimuli used in this study. Although no main effect of sex was detected in studies looking at immediate-early gene expression induced by different playback conditions (conspecific or heterospecific songs, male or female calls; Bailey and Wade, 2005; Scully et al., 2017), other salient stimuli might induce sex-specific responses. Indeed, bird's own song and tutor's song seem to induce smaller (however nonsignificant) NCM activation in males compared to novel conspecific songs (Terpstra et al., 2004) while in females, father's song induces a greater activation in NCM (Terpstra et al., 2006). Looking at the activation in response to father song could thus be interesting for future considerations, especially in the context of sex differences. Father's song might induce a differential activation in NCM aromatase neurons in males compared to females.

Topography of NCM

We observed a lower number of aromatase positive cells and a greater song-induced EGR1 expression in the dorsal part of NCM as compared to the ventral part. The differential activation between subregions of NCM has been previously observed (Sanford et al., 2010; Scully et al., 2017), and we build on this evidence to report differences in aromatase expression between dorsal and ventral NCM. Interestingly, the percentage of aromatase neurons detected by both the rabbit (Ikeda et al., 2017) and the sheep antibodies (present study) was slightly higher in the ventral NCM compared to the dorsal NCM (90.5% in vNCM, 86.5% in dNCM) which could partially account for this region-dependence. The dorsal NCM is also known to contain more cells as shown by DAPI staining (Vahaba et al., 2020) and confirmed in the present study that could explain the lower proportion of aromatase positive cells while the raw number between dNCM and vNCM might be similar.

This study further revealed a higher activation of aromatase cells in the dorsal part of NCM as compared to ventral NCM, suggesting that the dorsal NCM might be particularly important for local aromatization and estradiol-dependent song processing. This hypothesis is in agreement with previously published data showing a higher song-induced EGR1

expression in the dorsal NCM and that the estradiol-induced song selectivity (higher EGR1 response for songs over tones) was stronger in the dorsal NCM as compared to the ventral (Sanford et al., 2010). Furthermore, recent evidence shows that the dorsal NCM is specifically sensitive to the effect of aromatase blockade in the control of song-induced EGR1 expression (Krentzel et al., 2020). Extracellular recordings in European starlings reveal that neurons from the ventral NCM respond more strongly to unfamiliar songs (Thompson and Gentner, 2020). Further work on the distinction between ventral versus dorsal NCM are needed to define the region-dependent functional roles and modulatory events that support song processing.

Hemisphere similarities

The absence of lateralization in the current immunostaining study confirmed previous studies looking at aromatase expression (Ikeda et al., 2017; Saldanha et al., 2000) and song-induced EGR1 expression (Scully et al., 2017) within NCM. Our electrophysiological data however, indicated few lateralized features, with the exceptions being that tonic cells show smaller duration of evoked-spike and a faster recovery to resting state in the left hemisphere as compared to the right.

This result adds to a large literature on lateralization of the auditory forebrain of songbirds and other vocal learning species. The left hemisphere Wernicke's area of humans is dominant for language processing (Doupe and Kuhl, 1999; Price, 2012) and is considered a functional analog of the songbird NCM (Bolhuis et al., 2010; Jarvis, 2004). In songbirds, lateralization of song learning in the developing brain have emerged in studies of immediate early gene expression (Avey et al., 2005; Chirathivat et al., 2015; Moorman et al., 2015, 2012; Olson et al., 2016), electrophysiological recordings (Bell et al., 2015), epigenetic markers (Phan et al., 2017), and neurogenesis (Tsoi et al., 2014). Fewer studies have observed lateralization in the context of song processing in the adult brain. The left hemisphere was shown to have a higher song-induced EGR1 expression (Lampen et al., 2017) although this results was not observed in other studies (Chen et al., 2017; Scully et al., 2017). Blockade of aromatase rapidly disrupted male's song preference and it was observed only when the drug was infused in the left hemisphere (Remage-Healey et al., 2010). A more recent FMRI study corroborated this finding, showing that auditory-evoked activation was attenuated in the NCM of male European starlings when estrogen synthesis was blocked, and only in the left hemisphere (De Groof et al., 2017). Finally, the testosterone-mediating elevation in estradiol withinin NCM in response to song only occurs in the left hemisphere of female zebra finches (de Bournonville et al., 2020). Altogether, these data highlight the left hemisphere dominance for song processing and the crucial role of neurosteroids in the left NCM for this process.

The absence of lateralization in the song-induced EGR1 expression from the current data and previous studies (Chen et al., 2017; Scully et al., 2017) could be because EGR1 expression in NCM was not subdivided by cell type (beyond aromatase expression). Establishing whether the song-induced activation of aromatase cells only involves, e.g., tonic cells would be of great interest but would likely necessitate in vivo whole cell recordings. Finally, sustained spiking activity has been correlated to the processing of long-syllables and

motifs that are found in zebra finch song (Terleph et al., 2007). If tonic spiking neurons are involved in this sustained representation, then the faster responses (smaller duration and faster recovery) found in tonic neurons from the left NCM could be an intriguing hemisphere-specific feature of song processing worth pursuing.

Conclusions

To our knowledge, only one previous study attempted to characterize the intrinsic electrophysiological properties of confirmed aromatase immunoreactive neurons (Cornil et al., 2004), and that analysis was restricted to three formally identified aromatase+ neurons. Despite this small sample, the conclusions of that study are in general accordance with our findings, namely that aromatase+ neurons exhibit intrinsic properties that are indistinct from aromatase- neurons in the same brain region. Although we do not report differences between aromatase+ and aromatase- neurons in terms of intrinsic excitability, these similarities in firing patterns to artificial current injection may mask subtle differences in ionic conductances and expression of ion-channel genes that could still account for the steroidogenic nature of aromatase+ neurons. Populations of granulosa cells in the human ovary show clear enrichment for calcium-activated potassium channels (Kunz et al., 2007b; Traut et al., 2009) as well as voltage-gated calcium channels (Agoston et al., 2004) that are proposed to enable a broad activation range to a variety of regulatory inputs for steroidogenic synthesis. Similar observations have been made in adrenal glomerulosa cells (Barrett et al., 2016; Rossier, 2016), and therefore subtle differences in neuroestrogenic cells in regions like NCM are likely present and warrant further investigation. Based on electrophysiological findings with adrenal glomerulosa and ovarian granulosa cells, the relationship between membrane potential and neurosteroidogenesis may be dynamic, under the control of balancing calcium and calcium-activated potassium conductances, and below the threshold of action potential initiation (Hattangady et al., 2016; Rossier, 2016). Moreover, assessing physiological differences among neurosteroid phenotypes using in vitro patch clamp recordings has substantial limitations, including the separation from other brain circuits, the potential for intrinsic plasticity, and the effects of ambient temperature on biophysical parameters (e.g., Alonso and Marder, 2019). Further study of subthreshold dynamics as well as pharmacological and gene-expression profiles *in vitro* and *in vivo* will enable more thorough characterization and network situation of aromatase neurons and their steroidogenic capacity.

Supplementary Material

Refer to Web version on PubMed Central for supplementary material.

Acknowledgments

We thank Colin Saldanha (American University) for generously providing the rabbit anti-aromatase antibody and Marcy Kingsbury for providing the sheep anti-aromatase antibody. Jim Chambers kindly provided assistance with confocal imaging. We also thank Matheus Macedo-Lima and Garrett Scarpa for their help during patch-clamp experiments and with the patch analysis code.

Funding:

This work was supported by the U.S. National Institutes of Health R01NS082179, and the Belgian American Education Foundation (BAEF).

Data availability statement:

Data available on request from the authors.

Abbreviation list

FI	Frequency/current slope
HW	Peak half-width
NCM	Caudomedial nidopallium
PB	Phosphate buffer
PBS	Phosphate buffer saline
PBT	Phosphate buffer triton
PFA	Paraformaldehyde
PPT	Patcher's Power Tools
Ri	Input resistance
RMP	Resting membrane potential
Tau	Membrane time constant
VI	Voltage-Current

References

Agoston A, Kunz L, Krieger A, Mayerhofer A, 2004. Two types of calcium channels in human ovarian endocrine cells: Involvement in steroidogenesis. J. Clin. Endocrinol. Metab 89, 4503–4512. 10.1210/jc.2003-032219 [PubMed: 15356055]

Alonso L, Marder E, 2019. Visualization of currents in neural models with similar behavior and different conductance densities. eLife 8, 1–28.

Avey MT, Phillmore LS, MacDougall-Shackleton SA, 2005. Immediate early gene expression following exposure to acoustic and visual components of courtship in zebra finches. Behav. Brain Res 165, 247–253. 10.1016/j.bbr.2005.07.002 [PubMed: 16095729]

Bailey DJ, Wade J, 2005. FOS and ZENK responses in 45-day-old zebra finches vary with auditory stimulus and brain region, but not sex. Behav. Brain Res 162, 108–115. 10.1016/j.bbr.2005.03.016 [PubMed: 15922071]

Balthazart J, Choleris E, Remage-Healey L, 2018. Steroids and the brain: 50 years of research, conceptual shifts and the ascent of non-classical and membrane-initiated actions. Horm. Behav 99, 1–8. 10.1016/j.yhbeh.2018.01.002 [PubMed: 29305886]

Barrett PQ, Guagliardo NA, Klein PM, Hu C, Breault DT, Beenhakker MP, 2016. Role of voltage-gated calcium channels in the regulation of aldosterone production from zona glomerulosa cells of the adrenal cortex. J. Physiol 594, 5851–5860. 10.1113/JP271896 [PubMed: 26845064]

Bell BA, Phan ML, Vicario DS, 2015. Neural responses in songbird forebrain reflect learning rates, acquired salience, and stimulus novelty after auditory discrimination training. J. Neurophysiol 113, 1480–1492. 10.1152/jn.00611.2014 [PubMed: 25475353]

Billing A, Correia M, Kelly D, Li G, Bergan J, 2020. Synaptic connections of aromatase circuits in the medial amygdala are sex specific. eNeuro in press.

Bolhuis JJ, Okanoya K, Scharff C, 2010. Twitter evolution: Converging mechanisms in birdsong and human speech. Nat. Rev. Neurosci 11, 747–759. 10.1038/nrn2931 [PubMed: 20959859]

Bolhuis JJ, Zijlstra GGO, Den Boer-Visser AM, Van Der Zee EA, 2000. Localized neuronal activation in the zebra finch brain is related to the strength of song learning. Proc. Natl. Acad. Sci. U. S. A 97, 2282–2285. 10.1073/pnas.030539097 [PubMed: 10681421]

Braun M, Ramracheya R, Bengtsson M, Zhang Q, Karanauskaite J, Partridge C, Johnson PR, Rorsman P, 2008. Voltage-Gated Ion Channels in Human Pancreatic Beta-Cells : Electrophysiological Characterization and Role in Insulin Secretion. Diabetes 57, 1618–28. 10.2337/db07-0991.M.B. [PubMed: 18390794]

Chen AN, Meliza XCD, 2018. Phasic and tonic cell types in the zebra finch auditory caudal mesopallium 1127–1139. 10.1152/jn.00694.2017

Chen Y, Clark O, Woolley SC, Woolley SC, 2017. Courtship song preferences in female zebra finches are shaped by developmental auditory experience 18–20.

Chirathivat N, Raja SC, Gobes SMH, 2015. Hemispheric dominance underlying the neural substrate for learned vocalizations develops with experience. Sci. Rep 5, 11359. 10.1038/srep11359 [PubMed: 26098840]

Comito D, Pradhan DS, Karleen BJ, Schlinger BA, 2016. Region-specific rapid regulation of aromatase activity in zebra finch brain. J. Neurochem 136, 1177–1185. 10.1111/jnc.13513 [PubMed: 26709964]

Cornil CA, Dalla C, Papadopoulou-Daifoti Z, Baillien M, Dejace C, Ball GF, Balthazart J, 2005. Rapid decreases in preoptic aromatase activity and brain monoamine concentrations after engaging in male sexual behavior. Endocrinology 146, 3809–3820. 10.1210/en.2005-0441 [PubMed: 15932925]

Cornil CA, de Bournonville C, 2018. Dual action of neuro-estrogens in the regulation of male sexual behavior. Gen. Comp. Endocrinol 256. 10.1016/j.ygcen.2017.05.002

Cornil CA, Leung CH, Pletcher ER, Naranjo KC, Blauman SJ, Saldanha CJ, 2012. Acute and specific modulation of presynaptic aromatization in the vertebrate brain. Endocrinology 153, 2562–2567. 10.1210/en.2011-2159 [PubMed: 22508515]

Cornil CA, Seutin V, Motte P, Balthazart J, 2004. Electrophysiological and neurochemical characterization of neurons of the medial preoptic area in Japanese quail (Coturnix japonica). Brain Res 1029, 224–240. 10.1016/j.brainres.2004.09.047 [PubMed: 15542078]

Dagostin AA, Lovell PV, Hilscher MM, Mello CV, Leão RM, 2015. Control of Phasic Firing by a Background Leak Current in Avian Forebrain Auditory Neurons. Front. Cell. Neurosci 9, 471. 10.3389/fncel.2015.00471 [PubMed: 26696830]

de Bournonville C, Ball GF, Balthazart J, Cornil CA, 2017. Rapid changes in brain aromatase activity in the female quail brain following expression of sexual behaviour. J. Neuroendocrinol 29, e12542. 10.1002/mrd.22357

de Bournonville C, Dickens MJ, Ball GF, Balthazart J, Cornil CA, 2013. Dynamic changes in brain aromatase activity following sexual interactions in males: Where, when and why? Psychoneuroendocrinology 38, 789–799. [PubMed: 22999655]

de Bournonville C, McGrath A, Remage-Healey L, 2020. Testosterone synthesis in the female songbird brain. Horm. Behav 121. 10.1016/j.yhbeh.2020.104716

De Groof G, Balthazart J, Cornil CA, Van der Linden A, 2017. Topography and Lateralized Effect of Acute Aromatase Inhibition on Auditory Processing in a Seasonal Songbird. J. Neurosci 37, 4243–4254. 10.1523/JNEUROSCI.1961-16.2017 [PubMed: 28314822]

Dickens MJ, Cornil CA, Balthazart J, 2011. Acute stress differentially affects aromatase activity in specific brain nuclei of adult male and female quail. Endocrinology 152, 4242–4251. 10.1210/en.2011-1341 [PubMed: 21878510]

Dickens MJ, de Bournonville C, Balthazart J, Cornil CA, 2014. Relationships between rapid changes in local aromatase activity and estradiol concentrations in male and female quail brain. Horm. Behav 65, 154–164. 10.1016/j.yhbeh.2013.12.011 [PubMed: 24368290]

Doupe AJ, Kuhl PK, 1999. BIRDSONG AND HUMAN SPEECH: Common Themes and Mechanisms. Annu. Rev. Neurosci 22, 567–631. 10.1146/annurev.neuro.22.1.567 [PubMed: 10202549]

Dutar P, Vu HM, Perkel DJ, 1998. Multiple Cell Types Distinguished by Physiological, Pharmacological, and Anatomic Properties in Nucleus HVc of the Adult Zebra Finch. J Neurophysiol 80, 1828–38. [PubMed: 9772242]

Hattangady NG, Karashima S, Yuan L, Ponce-Balbuena D, Jalife J, Gomez-Sanchez CE, Auchus RJ, Rainey WE, Else T, 2016. MUTATED KCNJ5 ACTIVATES THE ACUTE AND CHRONIC REGULATORY STEPS IN ALDOSTERONE PRODUCTION. J Mol Endocrinol 57, 1–11. 10.1530/JME-15-0324.MUTATED [PubMed: 27099398]

Herbison AE, Moenter SM, 2011. Depolarising and hyperpolarising actions of GABAa receptor activation on GnRH neurons : towards an emerging consensus. J Neuroendocr 23, 557–569. 10.1111/j.1365-2826.2011.02145.x.Depolarising

Ikeda MZ, Krentzel AA, Oliver TJ, Scarpa GB, Remage-Healey L, 2017. Clustered organization and region-specific identities of estrogen-producing neurons in the forebrain of Zebra Finches (Taeniopygia guttata). J. Comp. Neurol 525, 3636–3652. 10.1002/cne.24292 [PubMed: 28758205]

Jarvis ED, 2004. Learned Birdsong and the Neurobiology of Human Language. Ann N Y Acad Sci 1016, 749–777. 10.1196/annals.1298.038 [PubMed: 15313804]

Kabelik D, Schrock SE, Ayres LC, Goodson JL, 2011. Estrogenic regulation of dopaminergic neurons in the opportunistically breeding zebra finch. Gen. Comp. Endocrinol 173, 96–104. 10.1016/j.ygcen.2011.04.026 [PubMed: 21600208]

Kirchner MK, Foehring RC, Callaway J, Armstrong WE, 2018. Specificity in the interaction of high-voltage-activated Ca(2+) channel types with Ca(2+)-dependent afterhyperpolarizations in magnocellular supraoptic neurons. J. Neurophysiol 120, 1728–1739. 10.1152/jn.00285.2018 [PubMed: 30020842]

Krentzel AA, Ikeda MZ, Oliver TJ, Koroveshi E, Remage L, 2020. Acute neuroestrogen blockade attenuates song - induced immediate early gene expression in auditory regions of male and female zebra finches. J. Comp. Physiol. A 206, 15–31. 10.1007/s00359-019-01382-w

Krentzel AA, MacEdo-Lima M, Ikeda MZ, Remage-Healey L, 2018. A Membrane G-Protein-Coupled Estrogen Receptor Is Necessary but Not Sufficient for Sex Differences in Zebra Finch Auditory Coding. Endocrinology 159, 1360–1376. 10.1210/en.2017-03102 [PubMed: 29351614]

Kunz L, Roggors C, Mayerhofer A, 2007a. Ovarian acetylcholine and ovarian KCNQ channels: Insights into cellular regulatory systems of steroidogenic granulosa cells. Life Sci 80, 2195–2198. 10.1016/j.lfs.2007.01.022 [PubMed: 17300810]

Kunz L, Roggors C, Mayerhofer A, 2007b. Ovarian acetylcholine and ovarian KCNQ channels: Insights into cellular regulatory systems of steroidogenic granulosa cells. Life Sci 80, 2195–2198. 10.1016/j.lfs.2007.01.022 [PubMed: 17300810]

Lampen J, Jones K, Mcauley JD, Chang S, Wade J, 2014. Arrhythmic Song Exposure Increases ZENK Expression in Auditory Cortical Areas and Nucleus Taeniae of the Adult Zebra Finch 9. 10.1371/journal.pone.0108841

Lampen J, McAuley J, Chang S, Wade J, 2017. ZENK induction in the zebra finch brain by song: Relationship to hemisphere, rhythm, oestradiol and sex. J Neuroendocr 29, e12543. 10.1111/ijlh.12426

Macedo-Lima M, Boyd HM, Remage-Healey L, 2021. Dopamine D1 receptor activation drives plasticity in the songbird auditory pallium. J Neurosci

Macedo-lima M, Remage-healey L, 2020a. Hormones and Behavior Auditory learning in an operant task with social reinforcement is dependent on neuroestrogen synthesis in the male songbird auditory cortex. Horm. Behav 121, 104713. 10.1016/j.yhbeh.2020.104713 [PubMed: 32057821]

Macedo-lima M, Remage-healey L, 2020b. Hormones and Behavior Auditory learning in an operant task with social reinforcement is dependent on neuroestrogen synthesis in the male songbird auditory cortex. Horm. Behav 121, 104713. 10.1016/j.yhbeh.2020.104713 [PubMed: 32057821]

Maney DL, Cho E, Goode CT, 2006. Estrogen-dependent selectivity of genomic responses to birdsong 23, 1523–1529. 10.1111/j.1460-9568.2006.04673.x

Meitzen J, Weaver AL, Brenowitz EA, Perkel DJ, 2009. Plastic and Stable Electrophysiological Properties of Adult Avian Forebrain Song-Control Neurons across Changing Breeding Conditions 29, 6558–6567. 10.1523/JNEUROSCI.5571-08.2009

Mello CV, n.d. A Zebra Finch Expression Atlas [WWW Document]. https://doi.org/RRID:nif-0000–24345

Mello V, Clayton F, 1994. Song-induced ZENK Gene Expression in Auditory Pathways of Songbird Brain and Its Relation to the Song Control System 14.

Mello CV, Ribeiro S, 1998. ZENK Protein Regulation by Song in the Brain of Songbirds 438, 426–438.

Moorman S, Gobes SMH, Kuijpers M, Kerkhofs A, Zandbergen MA, Bolhuis JJ, 2012. Human-like brain hemispheric dominance in birdsong learning. Proc. Natl. Acad. Sci 109, 12782–12787. 10.1073/pnas.1207207109 [PubMed: 22802637]

Moorman S, Gobes SMH, Van De Kamp FC, Zandbergen MA, Bolhuis JJ, 2015. Learning-related brain hemispheric dominance in sleeping songbirds. Sci. Rep 5, 1–7. 10.1038/srep09041

Moorman S, Mello CV, Bolhuis JJ, 2011. Prospects & Overviews From songs to synapses: Molecular mechanisms of birdsong memory. Bioessays 33, 377–385. 10.1002/bies.201000150 [PubMed: 21381060]

Olson EM, Maeda RK, Gobes SMH, 2016. Mirrored patterns of lateralized neuronal activation reflect old and new memories in the avian auditory cortex. Neuroscience 330, 395–402. 10.1016/j.neuroscience.2016.06.009 [PubMed: 27288718]

Phan ML, Gergues MM, Mahidadia S, Jimenez-Castillo J, Vicario DS, Bieszczad KM, 2017. HDAC3 Inhibitor RGFP966 Modulates Neuronal Memory for Vocal Communication Signals in a Songbird Model. Front. Syst. Neurosci 11, 1–12. 10.3389/fnsys.2017.00065 [PubMed: 28154528]

Pitra S, Zhang M, Cauley E, Stern JE, 2019. NMDA receptors potentiate activity-dependent dendritic release of neuropeptides from hypothalamic neurons. J. Physiol 597, 1735–1756. 10.1113/JP277167 [PubMed: 30629746]

Price CJ, 2012. A review and synthesis of the first 20years of PET and fMRI studies of heard speech, spoken language and reading. Neuroimage 62, 816–847. 10.1016/j.neuroimage.2012.04.062 [PubMed: 22584224]

Remage-Healey L, Coleman MJ, Oyama RK, Schlinger B. a, 2010. Brain estrogens rapidly strengthen auditory encoding and guide song preference in a songbird. Proc. Natl. Acad. Sci. U. S. A 107, 3852–3857. 10.1073/pnas.0906572107 [PubMed: 20133597]

Remage-Healey L, Dong SM, Chao A, Schlinger BA, 2012. Sex-specific, rapid neuroestrogen fluctuations and neurophysiological actions in the songbird auditory forebrain. J. Neurophysiol 107, 1621–1631. 10.1152/jn.00749.2011 [PubMed: 22190616]

Remage-Healey L, Jeon SD, Joshi NR, 2013. Recent evidence for rapid synthesis and action of oestrogens during auditory processing in a songbird. J. Neuroendocrinol 25, 1024–1031. 10.1111/jne.12055 [PubMed: 23746380]

Remage-Healey L, Joshi NR, 2012. Changing neuroestrogens within the auditory forebrain rapidly transform stimulus selectivity in a downstream sensorimotor nucleus. J Neurosci 32, 8231–8241. 10.1523/JNEUROSCI.1114-12.2012 [PubMed: 22699904]

Remage-Healey L, Maidment NT, Schlinger BA, 2008. Forebrain steroid levels flucuate rapidly during social interactions. Nat Neurosci 11, 1327–1334. 10.1038/nn.2200. [PubMed: 18820691]

Rohmann KM, Schlinger BA, Saldanha CJ, 2006. Subcellular Compartmentalization of Aromatase Is Sexually Dimorphic in the Adult Zebra Finch Brain. J. Neurobiol 66, 677–686. 10.1002/neu [PubMed: 16688765]

Rossier MF, 2016. T-type calcium channel: A privileged gate for calcium entry and control of adrenal steroidogenesis. Front. Endocrinol. (Lausanne) 7, 1–17. 10.3389/fendo.2016.00043 [PubMed: 26869991]

Saldanha CJ, Tuerk MJ, Kim YH, Fernandes AO, Arnold AP, Schlinger BA, 2000. Distribution and regulation of telencephalic aromatase expression in the zebra finch revealed with a specific

antibody. J. Comp. Neurol 423, 619–630. 10.1002/1096-9861(20000807)423:4<619::AID-CNE7>3.0.CO;2-U [PubMed: 10880992]

Sanford SE, Lange HS, Maney DL, 2010. Topography of estradiol-modulated genomic responses in the songbird auditory forebrain. Dev. Neurobiol 70, 73–86. 10.1002/dneu.20757 [PubMed: 19885833]

Scully EN, Hahn AH, Campbell KA, Mcmillan N, Congdon JV, 2017. ZENK expression following conspecific and heterospecific playback in the zebrafinch auditory forebrain 331, 151–158. 10.1016/j.bbr.2017.05.023

Terleph TA, Mello CV, Vicario DS, 2007. Species Differences in Auditory Processing Dynamics in Songbird Auditory Telencephalon 1498–1510. 10.1002/dneu

Terpstra NJ, Bolhuis JJ, Den Boer-Visser AM, 2004. An analysis of the neural representation of birdsong memory. J. Neurosci 24, 4971–4977. 10.1523/JNEUROSCI.0570-04.2004 [PubMed: 15163689]

Terpstra NJ, Bolhuis JJ, Riebel K, Van Der Burg JMM, Den Boer-Visser AM, 2006. Localized brain activation specific to auditory memory in a female songbird. J. Comp. Neurol 494, 784–791. 10.1002/cne.20831 [PubMed: 16374807]

Thompson JV, Gentner TQ, 2020. Song Recognition Learning and Stimulus-Specific Weakening of Neural Responses in the Avian Auditory Forebrain 1785–1797. 10.1152/jn.00885.2009.

Traut MH, Berg D, Berg U, Mayerhofer A, Kunz L, 2009. Identification and characterization of Ca2+-activated K+ channels in granulosa cells of the human ovary. Reprod. Biol. Endocrinol 7, 1–10. 10.1186/1477-7827-7-28 [PubMed: 19133142]

Tsoi SC, Aiya UV, Wasner KD, Phan ML, Pytte CL, Vicario DS, 2014. Hemispheric asymmetry in new neurons in adulthood is associated with vocal learning and auditory memory. PLoS One 9, e108929. 10.1371/journal.pone.0108929 [PubMed: 25251077]

Vahaba DM, Hecsh A, Remage-healey L, 2020. Neuroestrogen synthesis modifies neural representations of learned song without altering vocal imitation in developing songbirds. Sci. Rep 1–24. 10.1038/s41598-020-60329-3 [PubMed: 31913322]

Vahaba DM, Remage-Healey L, 2018. Neuroestrogens rapidly shape auditory circuits to support communication learning and perception: Evidence from songbirds. Horm. Behav 104, 77–87. 10.1016/j.yhbeh.2018.03.007 [PubMed: 29555375]

Vallentin D, Kosche G, Lipkind D, Long MA, 2016. Inhibition protects acquired song segments during vocal learning in zebra finches. Science 351(6270), 267–271. [PubMed: 26816377]

Vates GE, Broome BM, Mello CV, Nottebohm F, 1996. Auditory pathways of caudal telencephalon and their relation to the song system of adult male zebra finches (Taenopygia guttata). J. Comp. Neurol 366, 613–642. 10.1002/(SICI)1096-9861(19960318)366:4<613::AID-CNE5>3.0.CO;2-7 [PubMed: 8833113]

Woolley SMN, Gill PR, Fremouw T, 2009. Functional Groups in the Avian Auditory System 29, 2780–2793. 10.1523/JNEUROSCI.2042-08.2009

Yague JG, Muñoz A, De Monasterio-Schrader P, DeFelipe J, Garcia-Segura LM, Azcoitia I, 2006. Aromatase expression in the human temporal cortex. Neuroscience 138, 389–401. 10.1016/j.neuroscience.2005.11.054 [PubMed: 16426763]

Zengin-toktas Y, Woolley SC, 2017. Singing modulates parvalbumin interneurons throughout songbird forebrain vocal control circuitry 1–16. 10.1371/journal.pone.0172944

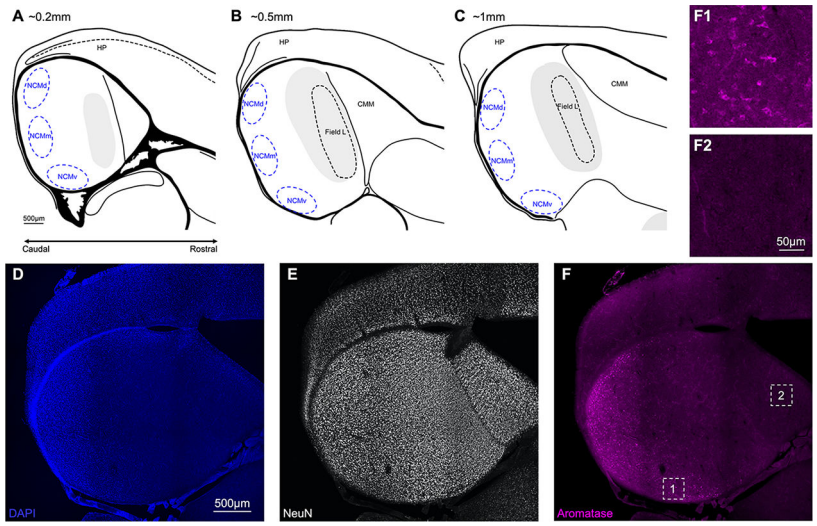

Figure 1:

Schematic representation and illustrative example of NCM sections. Illustrations of sagittal NCM sections medial (left) to lateral (right) (A-C; ~0.2–1.0 mm from midline; Modified from (Mello, n.d.) ZEBrA: A Zebra Finch Expression Atlas, RRID: nif-0000–24345; http://www.zebrafinchatlas.org). Blue dashed circles are approximate areas where 60x images were taken for quantifying aromatase and EGR1 positive cells in the dorsal (NCMd), medial (NCMm) and ventral NCM (NCMv). Illustrative example of 10X stitch NCM sections stained with DAPI (blue), NeuN antibody (white) and aromatase antibody (purple) (D-F) with zoomed regions showing neurons expressing aromatase in NCMv (F1) and CMM, a region with no reported aromatase somas (F2). Abbreviations : HP, Hippocampus; CMM, Caudal Medial Mesopallium.

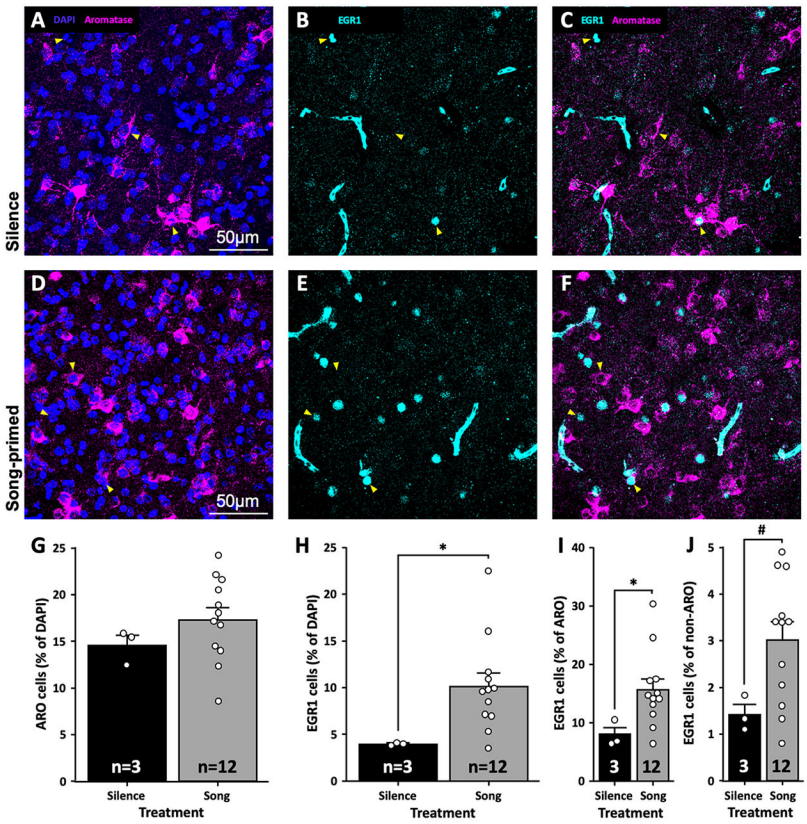

Figure 2:

Song-induced EGR1 expression in NCM aromatase neurons. Representative examples of aromatase positive cells (A, D, magenta), EGR1 positive cells (B, E, cyan) and the coexpression between both markers (C, F) within NCM of zebra finches exposed to silence (A-C) or song (D-F). The quantifications (G-J) showed an equivalent number of aromatase positive cells between groups (G) but a higher number of EGR1 neurons and coexpression in song primed-animals as compared to silence exposed animals (H-J). The three yellow arrows are pointing to the three cellular types (aromatase+ only, EGR1+ only and a cell that expresses both markers). Individual data are shown by the open circles. * $p<0.05$; # $p<0.1$.

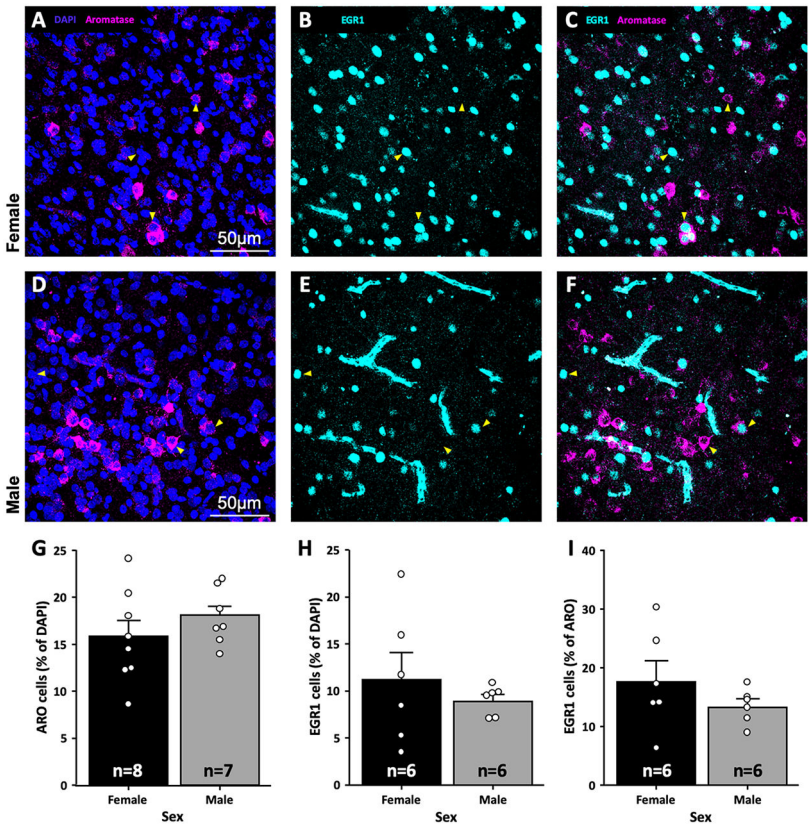

Figure 3:

Comparison between males and females of the song-induced EGR1 expression in NCM aromatase neurons. Illustrative examples of aromatase positive cells (A, D, magenta), EGR1 positive cells (B, E, cyan) and the coexpression between both markers (C, F) within NCM of females (A-C) and males (D-F). The quantifications of all markers (G-I) showed an equivalent expression between both sexes. The three yellow arrows are pointing to the three cellular type (aromatase+ only, EGR1+ only and a cell that expresses both markers). Individual data are shown by the open circles.

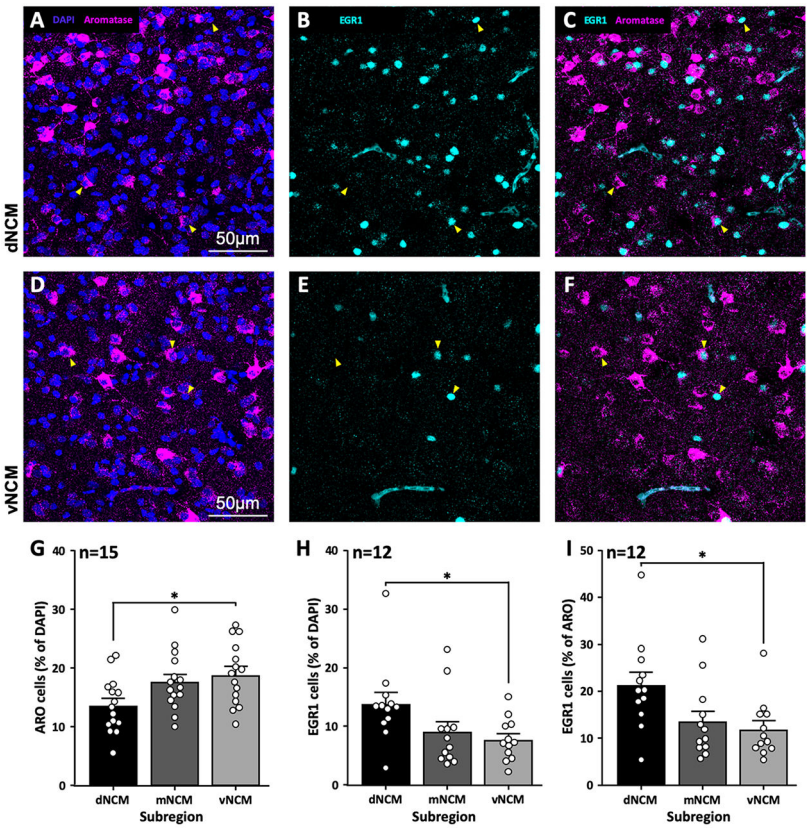

Figure 4:

Topography of the song induced-EGR1 expression in NCM aromatase neurons. Representative examples of aromatase positive cells (A, D), EGR1 positive cells (B, E) and the coexpression between both markers (C, F) in subregions of NCM. The quantifications demonstrated a higher number of aromatase positive cells in the ventral part of NCM as compared to the dorsal part (G). EGR1 expression (H) and EGR1 expression in aromatase positive neurons (I) was higher in the dorsal NCM as compared to the ventral NCM. The three yellow arrows are pointing to the three cellular type (aromatase+ only, EGR1+ only and a cell that expresses both markers). Individual data are shown by the open circles. * $p<0.05$.

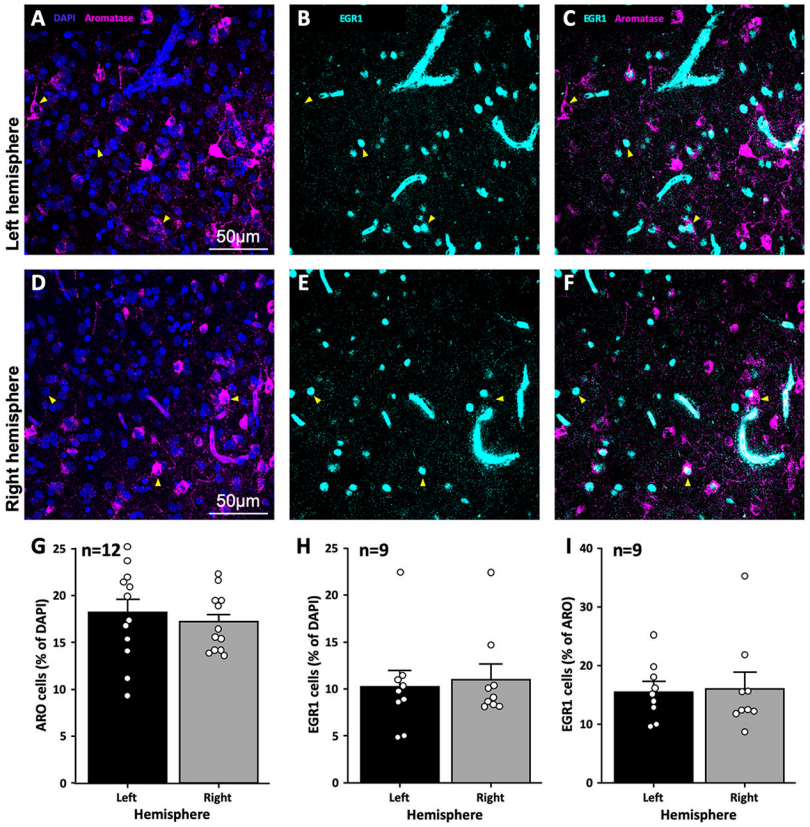

Figure 5:

Song induced-EGR1 expression in NCM aromatase neurons is similar in left and right hemispheres. Representative examples of aromatase positive cells (A, D), EGR1 positive cells (B, E) and the coexpression between both markers (C, F) in the left (A-C) and right (D-F) NCM. The quantifications demonstrated no differences between hemispheres for any of the three measures (G-I). The three yellow arrows are pointing to the three cellular types (aromatase + only, EGR1+ only and a cell that express both markers). Individual data are shown by the open circles.

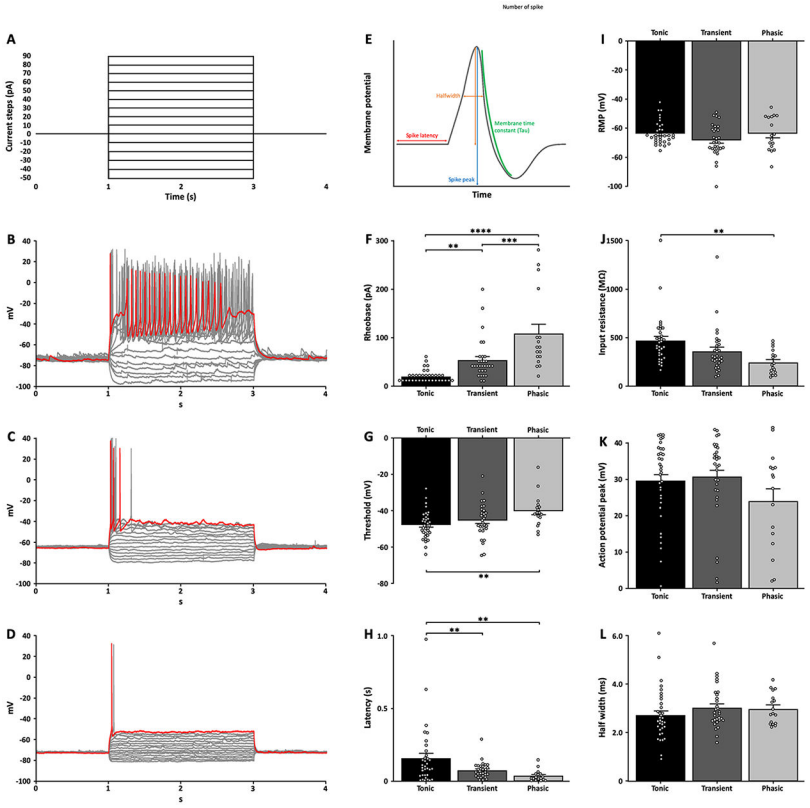

Figure 6:

Action potential and passive membrane properties of three neuronal phenotypes in NCM. Current steps protocols (A) and representative responses observed in cells defined as tonic (B), transient (C) and phasic (D) based on the number of action potentials. Intrinsic properties of action potential (E) quantified and compared between the different phenotypes. Rheobase (F), threshold (G), peak latency (H) resting membrane potential (I), input resistance (J), peak amplitude (K), and peak half width (L) of tonic, transient and phasic neurons. Individual data (neurons) are shown by the open circles. ** $p < 0.01$; *** $p < 0.001$; **** $p < 0.0001$.

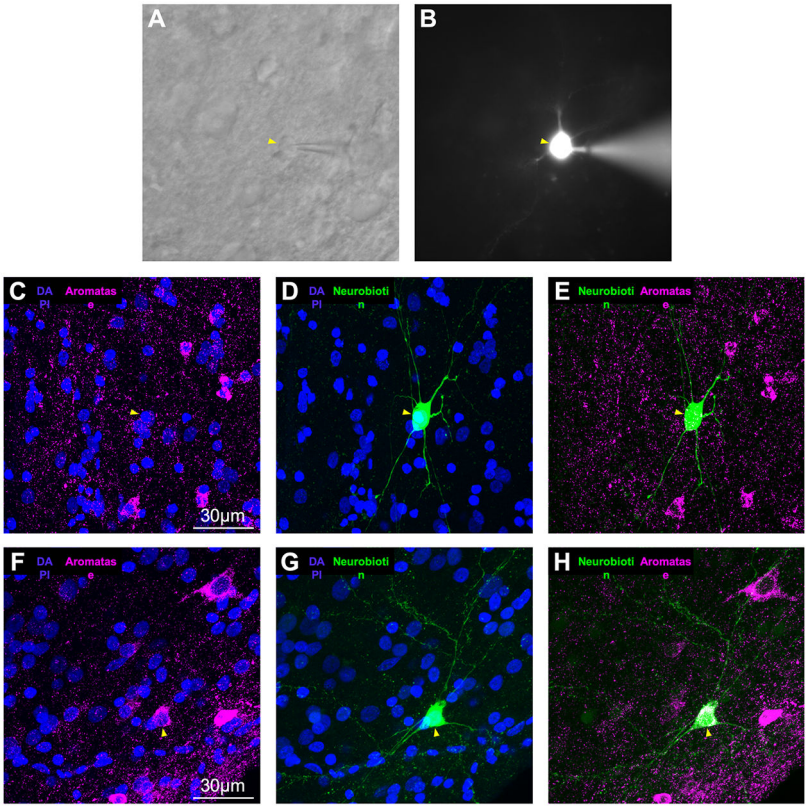

Figure 7:

Whole-cell patch clamp recordings and subsequent identification of NCM neurons. Visualization of an NCM neuron on the recording stage and the glass pipette approaching the neuron using DIC optics (A). Visualization of the same neuron filled with Alexa-488 contained in the internal solution (B). Subsequent identification of the same neuron as in A-B (C-E); i.e. picture of the patched neuron (D; Alexa-488 + streptavidin-488, green) and the absence of immunostaining for aromatase (C, magenta) confirmed by the overlay image (E). Example of a patched aromatase positive neuron (F-H)

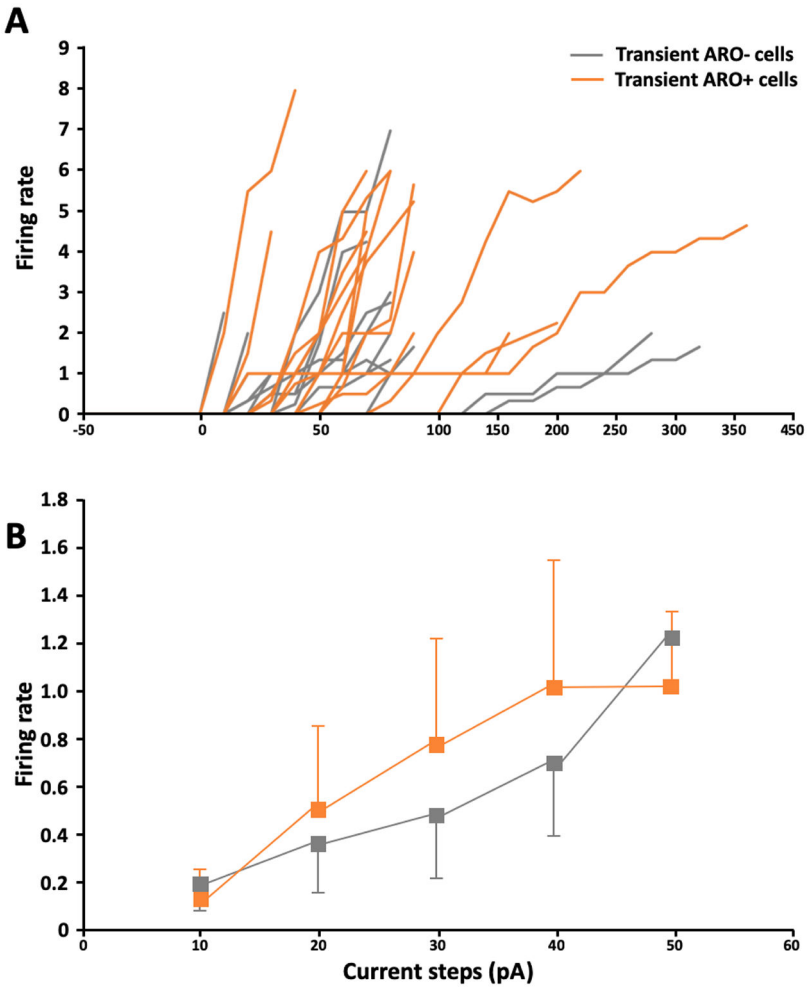

Figure 8:

Evoked firing rate of zebra finch NCM transient neurons expressing aromatase (orange) or not (gray). (A) Evoked firing rate and injected current (FI) curves of transient NCM neurons is not different between aromatase positive and aromatase negative neurons. (B) Mean evoked firing rate to positive currents do not differ between aromatase positive and aromatase negative neurons.

Table 1:

Intrinsic properties of aromatase positive (ARO+) vs. aromatase negative (ARO-) neurons of NCM

	Tonic		Transient		Phasic	
	ARO−	**ARO+**	**ARO−**	**ARO+**	**ARO−**	**ARO+**
Nb of cells	20	14	14	16	10	7
Nb of action potential	21.8 ± 3.3	24.6 ± 7.3	**3.9 ± 0.6**	**6.4 ± 0.6** **	n.a.	n.a.
RMP (mV)	−64.1 ± 1.9	−63.0 ± 2.3	−67.0 ± 3.6	−69.3 ± 2.3	−60.8 ± 3.3	−67.9 ± 4.8
Rheobase (pA)	20.5 ± 3.3	16.4 ± 2.2	52.9 ± 14.9	53.1 ± 6.9	95.0 ± 22.3	125.7 ± 36.8
Input resistance (MΩ)	470.1 ± 61.5	466.7 ± 57.4	359.0 ± 82.6	363.9 ± 39.1	266.7 ± 44.5	215.1 ± 35.9
Threshold (mV)	−48.7 ± 1.4	−46.0 ± 2.4	−47.0 ± 2.4	−41.0 ± 3.4	−39.9 ± 3.3	−39.9 ± 2.6
Peak amplitude (mV)	31.7 ± 2.4	26.3 ± 3.0	26.8 ± 2.8	34.0 ± 3.0	24.8 ± 4.6	24.1 ± 5.5
Peak latency (s)	0.14 ± 0.03	0.19 ± 0.07	0.08 ± 0.02	0.08 ± 0.01	0.04 ± 0.01	0.03 ± 0.01
Peak HW (ms)	2.5 ± 0.2	3.0 ± 0.3	3.1 ± 0.2	3.0 ± 0.2	3.1 ± 0.2	2.8 ± 0.2
Tau (ms)	2.3 ± 0.2	3.0 ± 0.5	2.9 ± 0.2	2.6 ± 0.2	2.7 ± 0.2	2.6 ± 0.2

Data expressed as mean ± SEM;

** $p < 0.01$ compared to ARO−